Microseismic moment tensors: A path to understanding frac growth

ADAM BAIG and TED URBANCIC, Engineering Seismology Group Canada

Microseismic monitoring is a valuable tool in understanding the efficacy of hydraulic fracture treatments. Determination of event locations and magnitudes leads to estimations of the geometry of the fracture zone and certain dynamics of the fracturing process. With sufficient resolution, the hypocenters may even reveal failure planes or other underlying structures controlling the distribution of events and of interest to petroleum engineers to test various hypotheses on fracture growth.

However, inverting for the moment tensor distribution opens up new dimensions in understanding the processes underlying the fracturing as it is a direct representation of the strain in the immediate vicinity of the source. The properties of the seismic moment tensor allow the orthogonal strain axes to be estimated for each event, and we can use that deformation information to identify the state of stress in the vicinity of the treatment and the potential failure planes. From there, we can examine a canonical problem in earthquake seismology: that of determining the orientation of the fault plane from a moment tensor. The fault-plane solution is an approximation of the moment tensor that assumes that deformation follows a double-couple shear model, but the symmetry of the solution admits two orthogonal solutions for the fault plane orientation. Using the strain axes of an ensemble of events with constraints to the stress field can help to resolve this ambiguity in fault orientation as one possible fault plane will be more consistent with the overall state of stress than the other. Therefore, we can determine the underlying fracture geometries independent of event locations contributing additional constraints to the resolution of the fracture network.

The full moment tensor, especially for microseismicity induced by hydraulic fracturing or other injection treatments, can be used to identify the volumetric failure mechanisms of events. One decomposition of these mechanisms partitions the moment tensor in three components: a double-couple component; an isotropic component that describes the volumetric strain (i.e., explosive or implosive); and a compensated linear vector dipole that describes strain in one sense along one axis and strain in the other sense along the other two (crack opening or crack closure). If we assume that the volumetric strain is in response to fluids, then we can begin to think about tracking the flow of proppant through the system by determining the volumetric deformation through the isotropic component of the moment tensor.

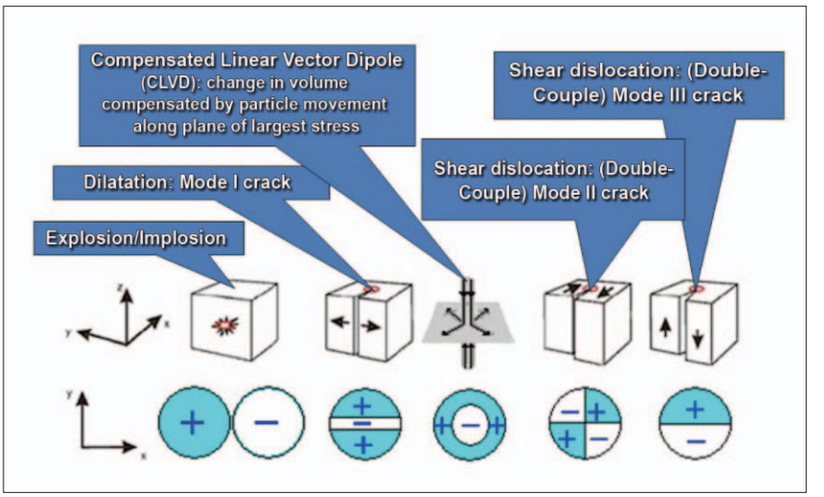

Figure 1. *Different modes of failure produce different moment tensors visualized though the "beach ball" diagrams, which are stereographic projections of the P-wave radiation patterns over the focal sphere.*

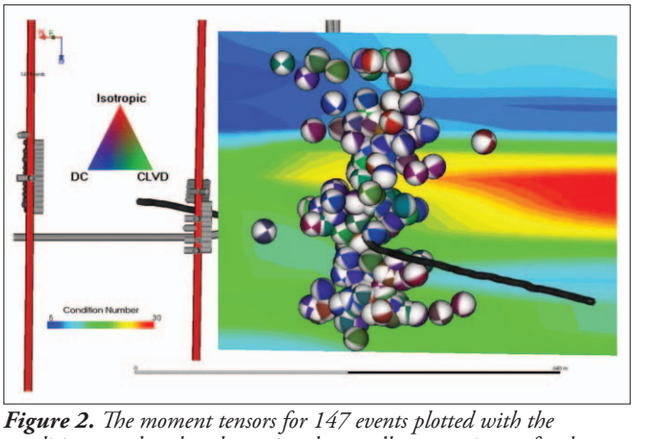

Figure 2. *The moment tensors for 147 events plotted with the condition number that determines how well one can invert for the mechanism of the event. The moment tensors are shown as beach balls colored by the proportion of double-couple, compensated linear vector dipole, and isotropic components according to the color triangle. Also shown is the treatment well (gray), the observation wells (red), and the triaxial sensors (the triads of gray cylinders).*

Moment tensors

The seismic moment tensor (SMT) is a symmetric, rank 2 tensor, which therefore has six independent components. The SMT is responsible for the observed radiation pattern from the event; mapping the total amplitudes (especially including the sense, positive or negative, of the first motion) of the P, SV, and SH phases to the focal sphere surrounding the source should determine this tensor, provided the sensor geometry is sufficiently well-distributed and the seismic data are high quality and properly modeled. For monitoring hydraulic fractures, full resolution of all six independent components requires that these total amplitudes be identified on at least two linear borehole arrays that are not coplanar with the event.

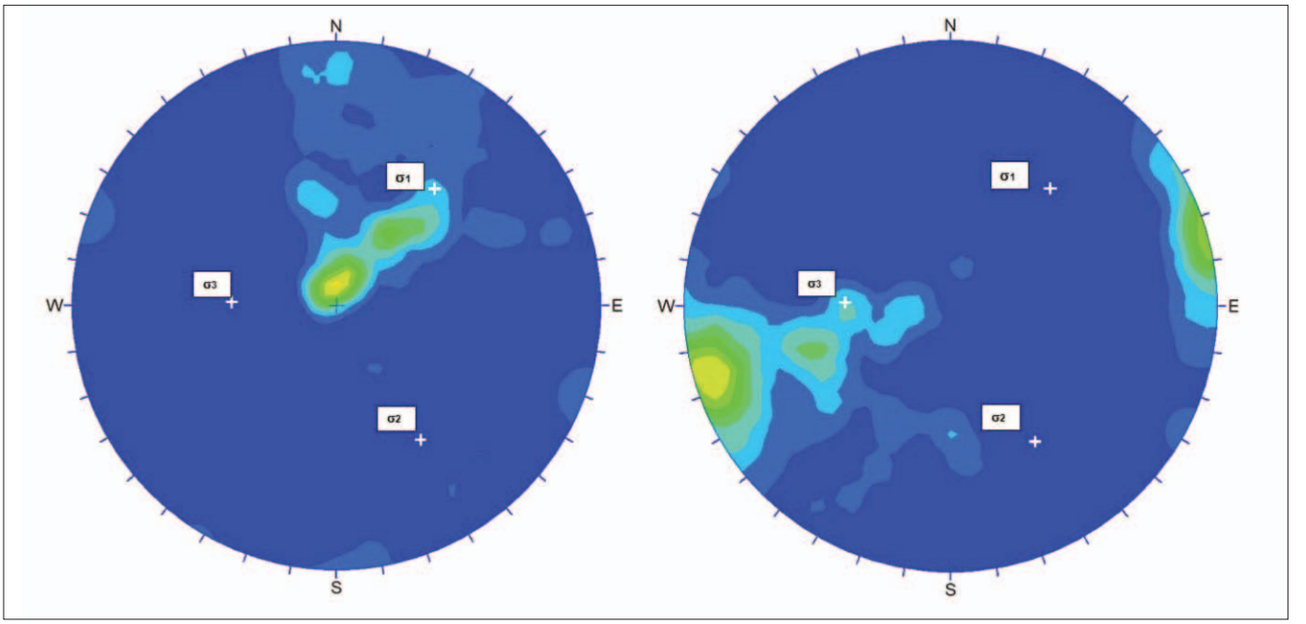

Figure 3. *Stereographic density plots of P axes (left) and T axes (right) for over 147 events recorded from a hydraulic fracture treatment. The principal stress axes determined from the algorithm of Gephart and Forsyth from this data set are overlain on both plots.*

Each SMT can be decomposed into six independent parameters: the three geometric parameters are controlled by the orientation of the fracture and the sense of slip thereon; one parameter is the total seismic moment (i.e., the strength of the event); and the other two control the relative strengths of the double-couple, compensated linear vector dipole and isotropic components. The non-double-couple modes of failure play an important role in elucidating the underlying failure mechanisms as they impart information about how the volume of the medium is changing in response to the treatment. Examples of the radiation patterns from various failure mechanisms are shown in Figure 1, and are related to various crack modes.

Determination of principal stress axes and fracture planes

As the SMT is a representation of strain at the source, with an ensemble of events each giving a measure of strain in the treatment zone, we can invert these strain axes for the stress regime that best fits these events. Gephart and Forsyth (1984) proposed an algorithm for realizing such an inversion for earthquake data in California. We can apply this method to microseismic data, by considering the double-couple approximations of the SMTs. The concept of this approach is not new for induced microseismicity. Urbancic et al. (1993) for example, applied this technique to mining-induced seismicity. The strain encoded in a moment tensor is frequently described by the P (pressure) and T (tension) axis of the event, which are simply the eigenvectors corresponding to the smallest and largest eigenvalues, respectively. With an ensemble of events, we can test various states of stress by determining the total rotations necessary to make the P and T axes of every event conform to the uniform test stress state; thus, the problem of determining the in-situ stress amounts to finding the state of stress that minimizes the total rotation of the strain axes from the ensemble of SMTs.

In Figure 2, we show the locations and moment tensor solutions for 147 events recorded utilizing three borehole arrays during a hydraulic fracture. The color scale of the events is controlled by the proportion of double-couple, compensated linear vector dipole, and isotropic components to the full source mechanism as prescribed with the color triangle. The events shown in the figure span an unusual vertical range of 500 m. Plotted behind the events is the condition number for the inversion to show the confidence that we have in the inversion of these moment tensors: the closer this number is to unity, the better constrained the inversion. In general, the observed low-condition numbers indicate that the obtained solutions are well-defined. The events themselves fall along a vertical plane trending N 40°E and feature a variety of mechanisms, suggesting that the events cannot be considered as simple shear failures but include volumetric components of failure.

In Figure 3, we show stereographic projections of the strain axes densities (pressure on the left, tension on the right) for a group of events recorded during the hydraulic fracture. Overlain as white crosses are the stress axes determined from the algorithm of Gephart and Forsyth. The trend of σ_1 is in agreement with the maximum horizontal shear stress observed from borehole strain measurements as well as being in agreement with the general trend of the events.

Double-couple moment tensors admit two orthogonal solutions for the fracture plane orientation. However, now that we can invert for the state of stress, for each event we can test these two candidate solutions: the plane that is most consistent with the state of stress is chosen for each event. Figure 4, on the left, shows a stereographic density plot for the poles of the best-fitting fracture planes determined from

the events from Figure 3. This plot reveals that these orientations fall into two groupings that are suborthogonal to each other. One explanation for this distribution is that the events are occurring along an en-echelon fracture network as shown on the right of Figure 4.

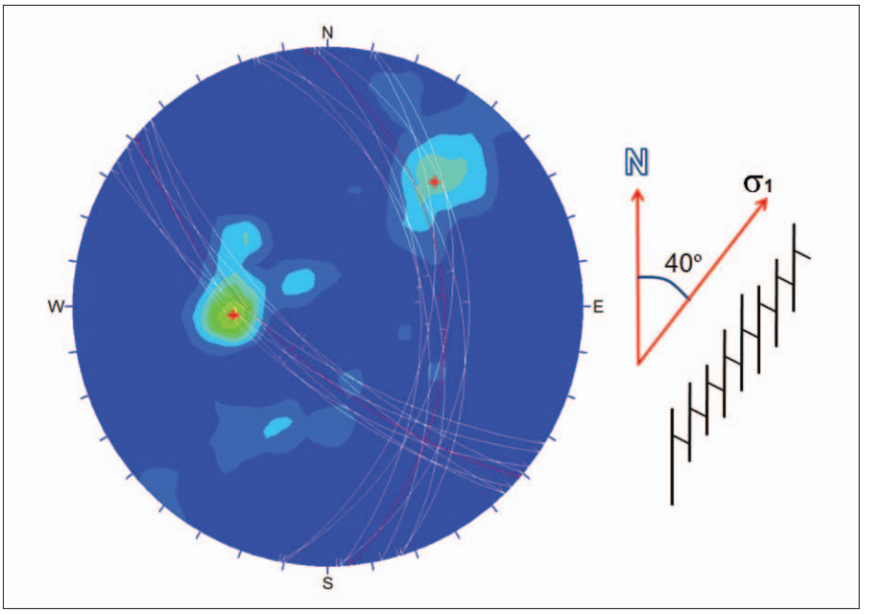

Figure 4. *(left) A stereographic density plot of the poles of the best-fitting fault planes from the 147 events in Figure 1. The red crosses mark the centers of the two main clusters in the density plot and are the poles to the red planes. The white planes give an indication of the amount of scatter in these best-fit planes. (right) An en-echelon model (in plan view) for the fracture propagation inferred from the stress distribution and the fracture planes.*

Non-double-couple components

Because of the injection of fluids and proppant, the assumption that the moment tensors are purely double-couple is too confining. Relaxing this restriction, there are generally two other modes of failure: a pure isotropic mechanism that corresponds to an implosion or explosion where all deformation is accommodated by a volumetric change, and a compensated linear vector dipole where strain along one axis is compensated by contraction or expansion along the other axes. In reality, we expect most moment tensors to be a hybrid of these three modes.

To parametrize the source type from the moment tensor, we note that the tensor has three real eigenvalues: m_1, m_2, and m_3. These eigenvalues determine the proportion of isotropic, compensated linear vector dipole, and double-couple contributions to the full moment tensor. The isotropic component is described by the trace of the tensor ($3m = m_1 + m_2 + m_3$) and the deviatoric moments are defined as:

$$m'_1 = m_1 - m \quad m'_2 = m_2 - m \qquad m'_3 = m_3 - m.$$

Following Hudson et al. (1989), we then order these deviatoric moments such that $|m'_1| < |m'_2| < |m'_3|$. This separation of the isotropic strain from the deviatoric allows the source type to be parameterized in terms of the quantities k and T, respectively:

$$k = \frac{m}{|m| + |m'_3|} \text{ and } T = \frac{2m'_1}{|m'_3|}$$

Both quantities vary between −1 and 1. A source with $k = 1$ corresponds to a purely explosive event, while one with $k = -1$ corresponds to a pure implosion. The $T \pm 1$ extremes are perhaps less easily envisioned, but correspond to sources where one strain axis is shortening while the other two are lengthening, or vice versa. All pure double-couple sources are uniquely described by $k = T = 0$. We note that all orientation information is not contained in this decomposition, because it relies only on the eigenvalues of the moment tensor.

The variety of source mechanisms can be discriminated in the source-type diagram (Figure 5) introduced by Hudson et al. In these plots, k, is on the vertical axis and the axis parallel to the top-right edge is T. The peculiar shape of this diagram is to ensure the even probability distribution of all source types. Double-couple mechanisms map to the center; purely explosive and implosive events are at the top and bottom of the diamond, respectively; and mechanisms corresponding to opening and closing of cracks translate to the top-right and bottom-left edges of the diagram.

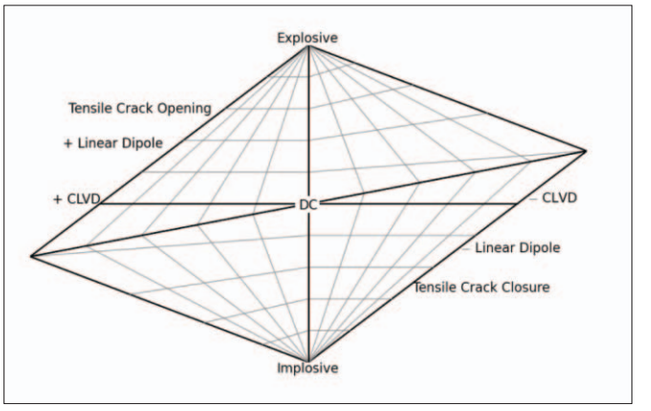

Figure 5. *A source-type diagram. In these plots, a mechanism will plot to different regions depending on the proportion of double-couple, compensated linear vector dipole, and isotropic contributions to the moment tensor. The sign of the compensated linear vector dipole and isotropic components is also distinguished here.*

In Figure 6, three such data sets from different treatments from separate wells in the same field are plotted. In the top left (red), there are a wide variety of mechanisms showing that the fracture is behaving in a very complex manner. To the top right (blue), the data are sparser, but there seems to be a small cluster of events representing crack openings and a larger cluster near the region of the diagram representing crack closures.

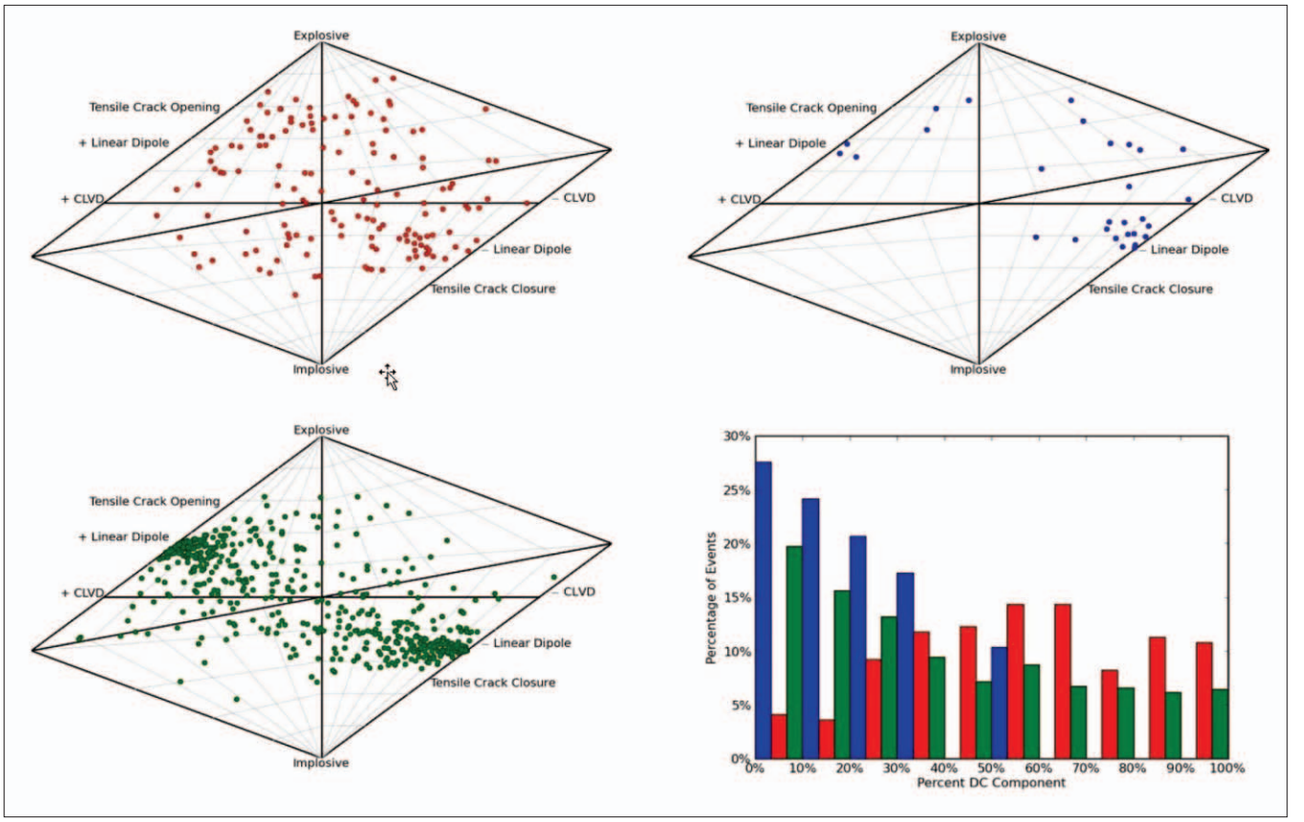

Figure 6. *Source-type diagrams for three treatments in different wells from the same field. In the lower right is a histogram of the proportion of events with a given amount of double-couple component for the three data sets; the color of the bars corresponds to the color of the point in the source-type plots.*

This type of pattern is seen in the lower-left source-type plot (green): events cluster on the poles of the axis between crack opening and closure. The difference in behavior of these data sets can be further illustrated in the histogram in the lower right. The higher proportion of double-couple events in the red data set would indicate that the events here are generated by a very different mechanism than the events in the other two data sets, possibly the re-activation of a pre-existing fault-fracture set resulting in a large amount of shear events. As these events were all recorded on multiple linear receiver arrays, moment tensor inversion condition numbers are similar to those shown in Figure 2.

Because of the wealth of events in the lower-left (green) data set, we can analyze it further and try to see if some coherent pattern emerges when plotted against the wellhead pressure and the total proppant pumped downhole. In Figure 7, we show four different windows of the treatment, roughly corresponding to different parts of the proppant volume curve. The first window (upper left) corresponds to the first injection of proppant (before this, not many events were observed); here the events concentrate to the crack opening axis of the source-type plots. The color scale of the events in the scatter plots shows that most events here are close to the well. After this first injection phase, most events still cluster to the crack opening axis with some events occurring farther away from the well. However, a significant number of events are starting to cluster around the crack closure axis, close to the well. The third interval corresponds to the start of a second phase of proppant injection. Events are still clustering to the poles of the crack opening/closure axis, but now the majority are closure-type failures. However, the same trend is observed in the locations of the events: the events are distributed even farther away from the well, with the farthest opening events still outpacing the closure events. Finally, at the end of the treatment, closure-type events are dominant. The farthest-out events in each phase of the treatment are progressing the fracture further away from the well and are uniformly crack-opening type mechanisms. Behind this fracture front, the region in the vicinity of the well shows a transition: initially fractures are expanded generating opening-type events and then relax back with closure-type mechanisms. There is also a closure front, defined by the maximum offset of the crack-closure events, behind the breakout front that progresses more slowly. These openings and closures tend to occur along similar fracture plane orientations

Thoughts

Monitoring microseismicity related to hydraulic fracture stimulations typically focuses on deriving event locations and the relative magnitude of events. As we have shown, a wealth of additional information can be obtained about the events themselves, and the conditions under which the events

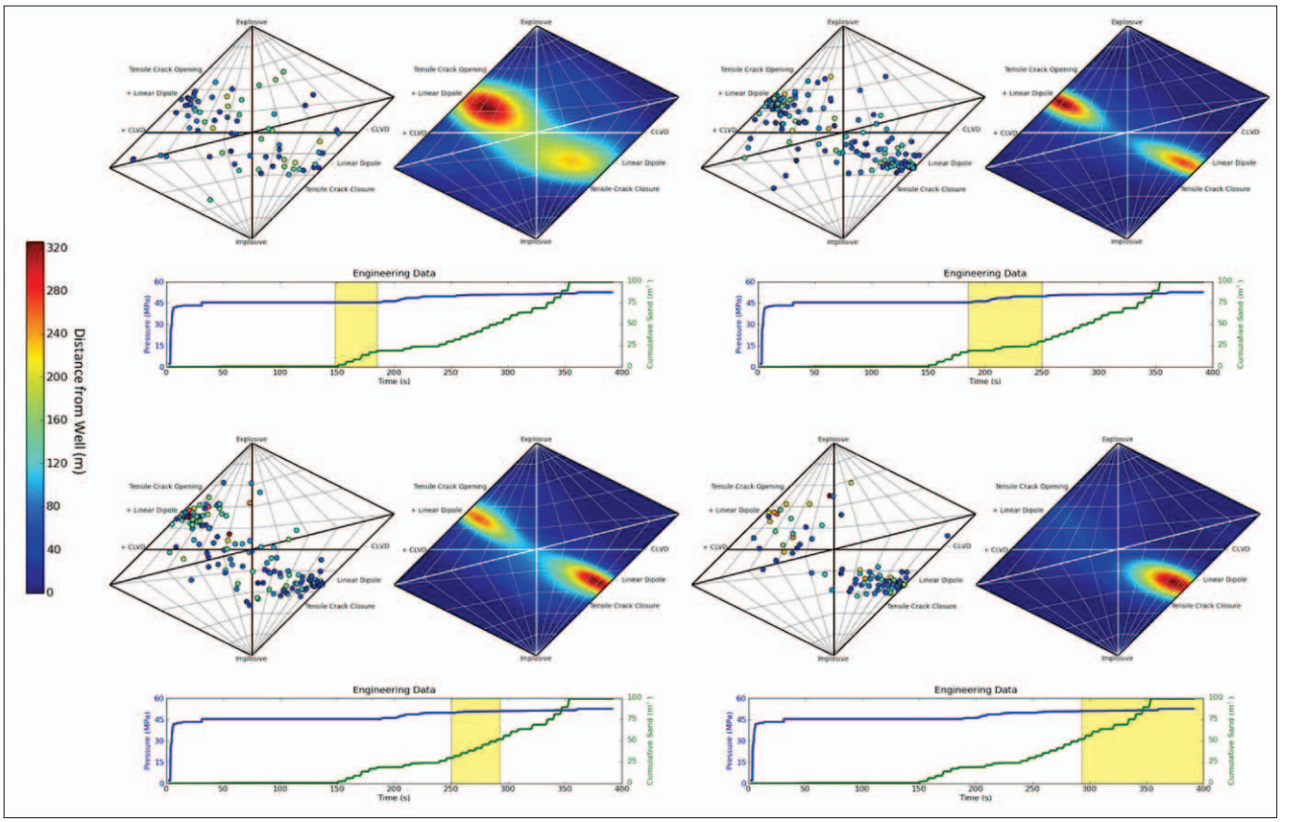

Figure 7. *For each quadrant, data from a different window of the treatment are plotted: (upper left) the scatter plot source-type diagram where each event is colored according to the horizontal distance from the treatment well (see color bar at far left); (upper right) a density contour plot of the same scatter plots, where red = an area of high density and blue = regions of few or no events; and (bottom) the time series of pressure and proppant volume with the time window, in yellow, of the data. The different quadrants correspond to (upper left) the beginning of the proppant injection; (upper right) a pause in the proppant injection; (lower left) the beginning of the next injection of proppant; and (lower right) the end of the treatment.*

are generated during the stimulation process, under appropriate monitoring conditions. Determining the stress-strain state and fracture orientations allows resolution of progressive fracture growth, such as we suggested by invoking an en-echelon fracture distribution along the maximum horizontal stress orientation. Further investigation of the individual strain components reveals the complexity of the individual failures but more importantly, by looking at the spatial and temporal variations of these failure components, a more definitive image of fracture development can be realized. The effective relation of pressure, proppant volume and rates, as seen, can be examined in the context of the observed seismic response, suggesting a direction for future assessment of the effectiveness of a treatment program. Further, it provides the opportunity to develop numerical models that can be used to predict the behaviour of the stimulation program. Of course, microseismic monitoring may then provide an approach to both validate and calibrate numerical models to enhance production. TLE

References

Ayers, W., T. I. Urbancic, and S. C. Maxwell, 2001, Passive microseismic monitoring to optimize well stimulation designs, SPE Annual Technical Conference and Exhibition, LA.

Gephart, J. and D. Forsyth, 1984, An improved method for determining the regional stress tensor using earthquake focal mechanism data: An application to the San Fernando earthquake sequence, *Journal of Geophysical Research*, 89, 9305–932.

Hudson, J., R. Pearce, and R. Rogers, 1989, Source type plot for inversion of the moment tensor, *Journal of Geophysical Research*, 94, 765–774.

Jost, M. and R. Hermann, 1989, A student's guide to and review of moment tensors, *Seismological Research Letters*, 60, 37–57.

Trifu, C-I., D. Angus, and V. Shumila, 2000, A fast evaluation of the seismic moment tensor for induced seismicity, *Bulletin of the Seismological Society of America*, 90, 1521–1527.

Urbancic, T. I., C-I. Trifu and R. P. Young, 1993, Microseismicity derived fault-planes and their relationship to focal mechanism, stress inversion, and geologic data, *Geophysical Research Letters*, 20, 2475–2478.

Acknowledgments: The authors thank their colleagues at ESG for their support and contribution to the studies. In particular, we thank Vladimir Shumila for his valuable discussions, and Sheri Bowman, Marc Prince, Lawrence Wamboldt, Keni Mallinen, Tiberius Trifu, Katherine Buckingham, Stephanie Alexander, Scott Valberg, and Christopher Orr for their invaluable input to the data analysis. Finally, the original manuscript was improved by comments from the guest editor and an anonymous reviewer.

Corresponding author: adam.baig@esg.ca